Title
Comparison between measurements of the poloidal distribution of magnetic fluctuations and predictions of theoretical models during TAE activity

Journal
Nuclear Fusion, 37(10)

ISSN
0029-5515

Authors
Heidbrink, WW
Jaun, A
Holties, HA

Publication Date
1997-10-01

DOI
10.1088/0029-5515/37/10/i07

COMPARISON BETWEEN MEASUREMENTS OF THE POLOIDAL DISTRIBUTION OF MAGNETIC FLUCTUATIONS AND PREDICTIONS OF THEORETICAL MODELS DURING TAE ACTIVITY

W.W. HEIDBRINK[a], A. JAUN[b], H.A. HOLTIES[c]
[a] University of California, Irvine, California, Unites States of America
[b] Alfvén Laboratory, Royal Institute of Technology, Stockholm, Sweden
[c] FOM Institute for Plasma Physics, Rijnhuizen, Nieuwegein, Netherlands

ABSTRACT. Fluctuations produced by beam-driven toroidicity-induced Alfvén eigenmode (TAE) activity in the DIII-D tokamak are measured by a poloidal array of magnetic probes and compared with the wavefields computed by two theoretical models. Fluid resistive models compute continuum damped TAEs. A kinetic plasma model that retains Landau damping and finite Larmor radius effects computes global drift-kinetic Alfvén eigenmodes. The phases of the probes disagree with both theoretical predictions, while the amplitudes agree best with the kinetic model.

1. INTRODUCTION

Toroidicity induced Alfvén eigenmodes (TAEs) are potentially dangerous instabilities that could be destabilized by alpha particles in a tokamak fusion reactor. Although there have been numerous measurements of the frequency and toroidal mode number of TAE activity [1], measurements of the radial and poloidal mode structure are relatively rare. Internal fluctuations are measured by reflectometer [2–4], soft X ray [5, 6] and electron cyclotron emission diagnostics but, because of the complex nature of the TAE eigenfunction, it is difficult to infer the mode structure from these measurements. The only published comparison of measurements of the mode structure with a theoretical prediction was performed by Durst et al. [7], who found that the poloidal mode number inferred from beam emission spectroscopy was consistent with the predictions of ideal MHD within ~50% uncertainties.

Despite the experimental difficulties, more accurate comparisons are highly desirable. There are a number of different theoretical predictions of the eigenfunction, each yielding different predictions for the stability threshold. The ideal MHD model [8] is widely employed, but both plasma kinetic [9–12] and energetic particle [11, 13–15] effects modify the predicted eigenfunction.

Magnetic probes are simple, sensitive diagnostics of TAE activity. This paper reports the first comparison of a poloidal array of probe measurements during TAE activity with theoretical predictions. We find that the wave fields at the edge are sensitive to the global eigenfunction predicted by the theoretical models, so the probe data are useful as a diagnostic of the mode structure. We also find that a model that includes kinetic effects gives better agreement with experiment than the resistive MHD models.

2. APPARATUS

For the comparison, we select a well documented, thoroughly analysed discharge, DIII-D shot 71 524 at 1875 ms. This is a low field (0.8 T), deuterium plasma of moderate elongation (1.6) that is limited on the inner wall and is heated by 5 MW of deuterium neutral beams. The flux surfaces and kinetic profiles appear in Figs 3 to 5 of Ref. [16], the Alfvén gap structure is illustrated in Fig. 3 of Ref. [17] and the time evolution of this discharge is shown in Refs [18, 19]. The TAE activity occurs in ~1 ms bursts separated by ~8 ms; the cycle resembles those shown in Ref. [20] and is caused by the loss of ~7% of the beam ions at each burst. Each burst contains a 'cluster' of several toroidal modes with mode numbers $n = 1$–9 [16]. The splitting of the peaks in the spectrum is caused by the Doppler shift [18]. For some of the bursts, each peak in the spectrum actually contains more than one toroidal mode [18].

A poloidal array of 21 probes at a single toroidal location measures the poloidal component of the magnetic field (Fig. 1). The probes consist of glass

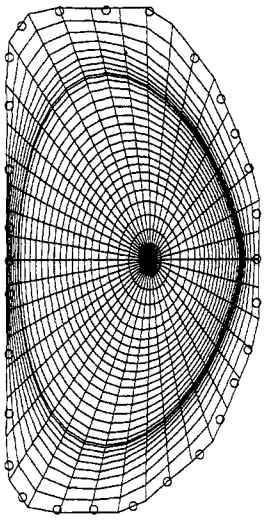

FIG. 1. Equilibrium mesh used in PENN to discretize the plasma cross-section and the surrounding vacuum region in real space; the circles correspond to the positions of the magnetic probes. (Only 21 of the 29 probes collected useful data for discharge 71 524.) The symmetry axis of the torus is on the left side of the figure.

cloth-insulated wire wound on a cylindrical ceramic spool, with each half of the array housed in a thin wall rectangular Inconel tube [21]. The distance of the probes from the graphite tiles is similar for all the probes in the array. The inductance of the coils varies between 92 and 125 μH, which is computed [21] to introduce negligible (<2°) variations in phase for the highest frequency modes considered here (94 kHz). Shorting between graphite tiles occurs occasionally and may introduce spurious phase differences for one or two probes in the array.

3. THEORETICAL MODELLING

Two wave codes featuring three different models for the linear plasma response are used in the comparisons. The CASTOR code [22] solves the linearized resistive MHD eigenequations using a Fourier decomposition poloidally and a combination of cubic and quadratic finite elements in the radial direction. It is well suited for the modelling of the fast magnetosonic and shear Alfvén waves when the temperature is sufficiently low that resonant surfaces absorb the power locally with resistive dissipation in a process commonly called continuum damping. In practice, the physical resistivity due to electron–ion collisions is small relative to neglected damping effects, so that higher values are used to resolve the sharp wavefield variations near the Alfvén resonances with the spatial discretization. In initial calculations with the 'antenna' version of CASTOR [23], the mode structure near the edge of the plasma (and therefore the magnetic field perturbations in the vacuum) depended on the choice of mode numbers excited with the antenna, so the 'linear stability' version of CASTOR is used here.

The PENN code [24] solves the Maxwell equations using cubic finite elements in the radial and poloidal directions. An oscillating helical source current is distributed inside the plasma to excite bulk modes which in the experiment are driven by the fast beam ions. Eigenmodes calculated in this manner are physically meaningful only if the damping is sufficiently small that the wavefield is independent of the excitation, which was indeed the case. The linear response of the plasma is defined in terms of a dielectric tensor featuring a resistive plasma model similar to the resistive model employed in CASTOR, and a kinetic finite Larmor radius (FLR) model that is appropriate for higher temperatures. By taking into account the FLR excursions, the drifts of thermal particles and the resonant Landau interactions, the kinetic model is not only well suited for the propagation of the fast waves, but it also models the linear mode conversion to the slower waves such as the kinetic Alfvén, the ion acoustic and the drift waves.

The effect of the energetic ions on the mode structure [11, 13–15] is neglected in both codes.

To compare theoretical eigenmode structures with measurements from a poloidal magnetic probe array, the position and orientation of the pick-up coils (Fig. 1) have been defined in the codes. The EFIT code [25] is used to reconstruct the equilibrium from the experimental data. For CASTOR, the EFIT equilibrium is recomputed using the HELENA code [26]. For PENN, an equilibrium is reconstructed [27] from the EFIT equilibrium, leading within the uncertainties in the diagnostics to a similar representation of the D-shaped high-β plasma. The low density region around the last closed magnetic surface is taken as a perfect vacuum, and the vessel is modelled as a perfectly conducting wall. For CASTOR, a Fourier series models the shape of the vacuum chamber. Since the coils are close to the wall, the magnetic field response is determined on the wall, at the poloidal angles that correspond to the coil positions. PENN uses the actual vacuum vessel segments in its modelling.

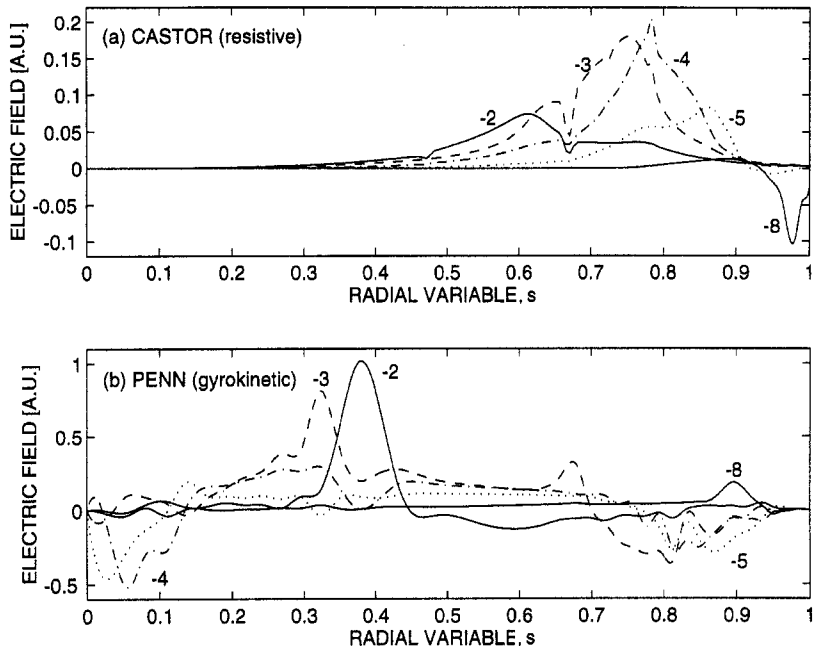

FIG. 2. Fourier components (continuous lines, −2 and −8; dashed line, −3; chain line, −4; dotted line, −5) of (a) the binormal electric field and (b) $\xi_\perp$ versus the square root of the normalized poloidal flux $s = \sqrt{(\Psi - \Psi_0)/(\Psi_1 - \Psi_0)}$ for the $n = 2$ mode found (a) at 56 kHz with CASTOR and (b) at 62 kHz with PENN.

4. RESULTS

To minimize numerical errors and maximize the sensitivity of the external measurements to the internal structure, we select low toroidal mode numbers ($n = 2, 3$) for the comparison. In the plasma frame, the measured frequency of the TAE is 64 kHz, with an uncertainty of ~4 kHz associated with the Doppler shift correction [18]. The variation in frequency between bursts is ~2 kHz.

The $n = 2$ CASTOR simulation finds an internal mode at 44 kHz, and an external mode at $f = 56$ kHz. The mode at 56 kHz is acceptably close to the observed mode frequency (uncertainties in the equilibrium reconstruction generate some uncertainty in the theoretical prediction), while the 44 kHz mode is not. The $n = 2$ kinetic PENN calculation includes perturbatively the drive from the fast beam ions and predicts an unstable mode at 62 kHz [12], in excellent agreement with the experiment.

Although the computed frequencies of the mode in the plasma frame are similar for the two codes, the mode structure calculated by the resistive CASTOR code differs considerably from the structure calculated by the kinetic version of PENN (Fig. 2). For PENN, the displacement is appreciable in the plasma interior and is largest on the low field side. For CASTOR, the TAE mode has its largest amplitude on the low field side but, since the wall (and the coils) on the high field side are closer to the plasma, a stronger magnetic perturbation is predicted for the inner coils. These differences stem from differing treatments of dissipation and mode coupling in the two models. To assess the effect of the dissipation model, a study was conducted with the resistive version of PENN, varying the shape of the arbitrarily chosen resistivity from constant throughout the plasma (assumed in the CASTOR calculation) to a hollow profile obtained by scaling the physical resistivity (defined by the electron–ion collision rate) by a non-physical multiplier. Apart from a decrease in the average resistivity and an increase in the eigenfrequency, the hollow profile also modifies the wavefield, which changes from peaked on the high field side of the plasma to dominant on the low field side. In addition to differences in the treatment of dissipation, the code predictions differ because the kinetic version of PENN includes mode coupling. In the core, coupling to drift waves is important [12]. In the edge, the radial separation of the gaps is comparable to the wavelength of kinetic Alfvén waves, so the coupling between poloidal harmonics

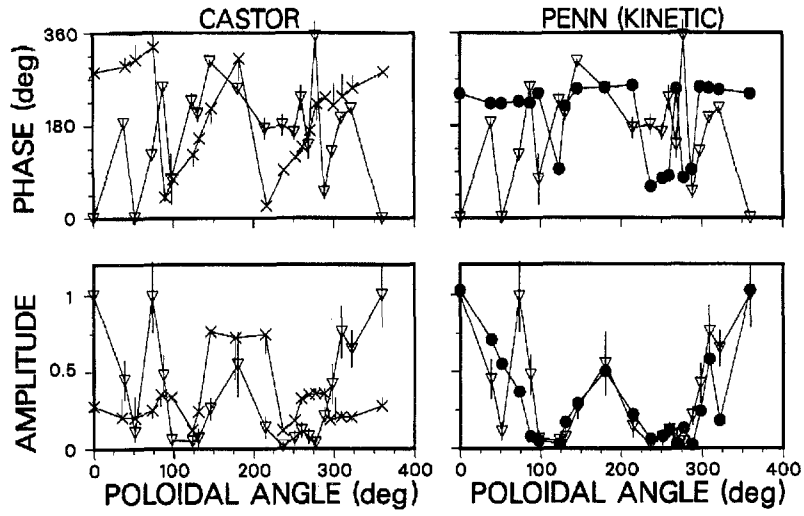

FIG. 3. Phase angle and relative amplitude of the magnetic fluctuations versus poloidal angle for the $n = 2$ mode. The poloidal angle increases anticlockwise around the vessel from 0° on the outer midplane (the low field side). The data (triangles) are compared with the predictions of the kinetic model of the PENN code (circles) and those of the resistive CASTOR code (crosses). The results of the sensitivity analysis are shown as lines extending from the CASTOR points. For the phase comparisons, the experimental phase is plotted relative to the probe at 0°; for the theories, the reference for the phase was varied to minimize χ^2. For the amplitude comparison, the amplitude is plotted relative to the probe at 0°; for the theories, the amplitudes are normalized so that the average amplitude is equal to the experimental average.

is altered by the inclusion of FLR effects [12]. In previous work, the eigenfunction was also computed by the ideal MHD codes GATO [17] and NOVA-K [28]. Like CASTOR, these fluid codes predict that the maximum amplitude of the eigenfunction occurs near $s = 0.75$.

For the $n = 2$ experimental data, two bursts at 1868 and 1885 ms with laboratory frequencies of 86.0 and 83.3 kHz are selected. (The burst at 1876 ms is excluded, because a fine structure of distinct, overlapping modes is observed [18].) The Fourier transform is computed using a 3 ms time window with 2 kHz smoothing in frequency; the data from the two bursts are then averaged for each probe (with each measurement weighted by the statistical uncertainty of the fast Fourier transform).

The data and the calculations are compared for the $n = 2$ mode in Fig. 3. The agreement with the relative phase is poor for both theoretical models. For the probe amplitude, the agreement is better for the kinetic PENN calculation than for the resistive CASTOR calculation. In particular, the data indicate that the mode is more strongly excited on the low field side of the plasma than on the high field side, in contradiction to the CASTOR prediction.

Because the theoretical calculations require large amounts of computer time, a detailed uncertainty analysis of the theoretical predictions is impractical. As an alternative, a new EFIT equilibrium that is barely consistent with the experimental data was constructed. (The q profile resembles curve E in Fig. 2(a) of Ref. [29], although the density was also perturbed to maximize the difference in $q/\sqrt{n_e}$ from the baseline case.) CASTOR then analysed the modified equilibrium. The predictions were affected by the change in the central q and density profiles (Fig. 3), although the qualitative features of the mode structure remained unaltered. For the purpose of estimating the uncertainty in a typical theoretical prediction, the computed probe data from the two runs are treated as an ensemble, yielding a variation of $24 \pm 13°$ in the predicted phase angle and a variation of $18 \pm 21\%$ in the relative amplitude.

Armed with an estimate of the theoretical uncertainty, it is possible to quantify the agreement between theory and experiment. For the phase

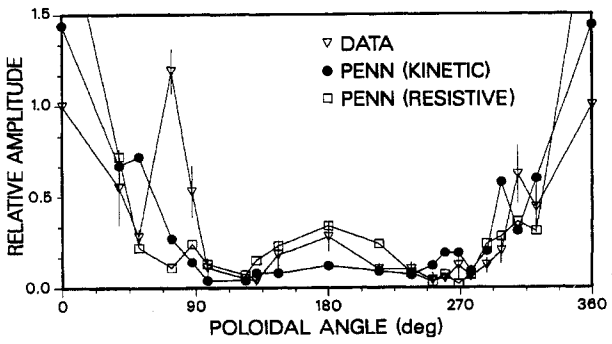

FIG. 4. Amplitude versus poloidal angle for the $n = 3$ mode. The theoretical predictions are from the PENN code using the kinetic (circles) and resistive (squares) models.

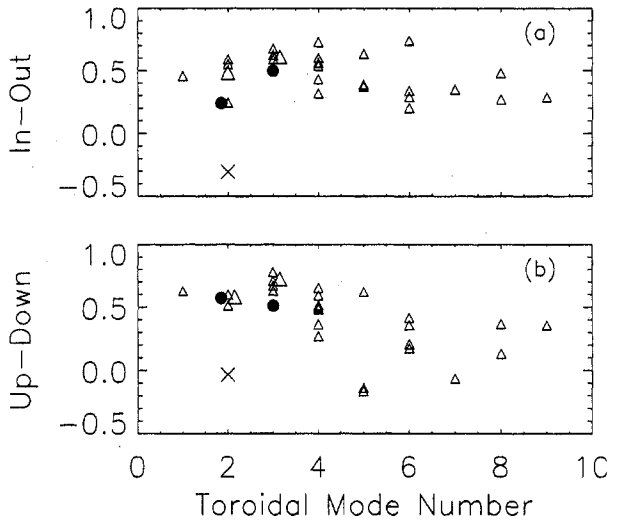

FIG. 5. Asymmetry of the relative amplitude versus toroidal mode number for 29 TAEs (triangles) in discharges similar to shot 71 524. The enlarged triangles represent the data shown in Figs 3 and 4; the theoretical predictions for CASTOR (crosses) and the kinetic version of PENN (circles) are also shown. (a) Horizontal asymmetry, $(\int_{-\pi/2}^{\pi/2} A\,\mathrm{d}\theta - \int_{\pi/2}^{3\pi/2} A\,\mathrm{d}\theta)/\int_0^{2\pi} A\,\mathrm{d}\theta$, where A is the amplitude. (b) Vertical asymmetry near the top and bottom of the vessel, $(\int_{3\pi/8}^{5\pi/8} A\,\mathrm{d}\theta - \int_{11\pi/8}^{13\pi/8} A\,\mathrm{d}\theta)/(\int_{3\pi/8}^{5\pi/8} A\,\mathrm{d}\theta + \int_{11\pi/8}^{13\pi/8} A\,\mathrm{d}\theta)$. The data for $n \geq 5$ are also vertically asymmetric, but the asymmetries do not necessarily appear near $\theta = \pm\pi/2$. All plotted data satisfy four criteria: (1) the discharge is from the same day as shot 71 524, (2) the mode frequency falls in the calculated TAE gap, (3) the data from the toroidal probe array only fit a single toroidal mode number (typically $\chi_r^2 \lesssim 0.2$) and (4) the coherence of all 21 probes in the poloidal array is $\gtrsim 0.4$.

difference between probes, the reduced chi squared χ_r^2 is 17 for CASTOR and 18 for PENN. For the relative amplitude, χ_r^2 is 2.4 and 1.2, respectively. Thus, for the relative amplitude, the kinetic PENN prediction is consistent with the experimental data while the CASTOR prediction is not. The phase predictions are inconsistent with experiment for both models.

A similar comparison has been carried out between the experimental data for the $n = 3$ mode and both the resistive and the kinetic PENN models (Fig. 4). Two bursts (94.9 kHz at 1868 ms and 93.6 kHz at 1884 ms) are apparently pure $n = 3$ modes. Once again, for both models, the predicted phase (not shown) bears no resemblance to the experimental values ($\chi_r^2 \simeq 6$). The kinetic prediction for the relative amplitude is somewhat better ($\chi_r^2 = 1.6$) than the resistive prediction ($\chi_r^2 = 2.0$), and does not depend on an arbitrary resistivity.

The generality of the data is assessed by analysing other discharges that resemble shot 71 524. (The toroidal field and current vary in these discharges, but the shape and wall conditions are similar.) Pure TAEs with reliable poloidal data are selected, then an interpolated curve is fitted to the poloidal distribution, and the horizontal and vertical asymmetries are computed. As shown in Fig. 5(a), the relative amplitude is largest on the outside of the tokamak for all of the analysed TAEs. The vertical asymmetries evident in Figs 3 and 4 are generally observed as well (Fig. 5(b)).

Independent information on the eigenfunction is provided by soft X ray measurements in a nominally identical discharge. Because of the complex spatial structure of the TAE eigenfunction, the chordal data are difficult to invert but, qualitatively, the displacement is largest (~0.5 mm) near $s = 0.4$, in rough agreement with the eigenfunction predicted by the kinetic version of PENN. A secondary peak of ~0.1 mm occurs near $s = 0.7$–0.8. The absolute magnitude of the soft X ray oscillation implies a maximum mode amplitude $\tilde{B}/B$ of $O(10^{-4})$. The measured fluctuation amplitude at the outer ($\theta = 0$) magnetic coil is $\tilde{B}/B = 2.5 \times 10^{-5}$; the kinetic PENN eigenfunction predicts a maximum internal amplitude 12 times larger, in rough agreement with the soft X ray data.

5. DISCUSSION AND CONCLUSIONS

Perhaps the most important finding of this study is that the external probe measurements are sensitive to global features of the eigenfunction. Alternative physical models give predictions that differ

appreciably (i.e. by much more than the experimental uncertainties in the probe data). Uncertainties in the equilibrium reconstruction yield uncertainties in the theoretical predictions that are comparable to the probe errors.

The theoretical predictions are in much better agreement for the amplitude than for the phase. The agreement with the phase data is very poor. From the experimental standpoint, there is no a priori reason to distrust the phase data in the 50–100 kHz frequency band. Perhaps inaccuracies in the modelling of the geometry near the probes have a greater impact on the phase predictions than the amplitude predictions. It is also possible that the discrepancy reflects actual deficiencies in the theoretical models.

There are several neglected effects that could be of importance. Dissipative effects are expected to have a greater impact on the predicted phase than on the mode amplitude. Another possibility is that the large beam ion population affects the mode structure. (The central fast ion pressure is ~45% of the total pressure [16].) Alternatively, the experimental modes may not really be pure eigenmodes, either owing to overlap of different modes in the experimental spectrum or to non-linear effects. (The codes compute the linear eigenfunction of a single eigenmode.) Saturation is thought to be governed by fast ion loss rather than mode coupling [20], but the excitation of several toroidal modes that rotate together [18] suggests that non-linear coupling occurs between modes. The mode amplitude in the plasma is only $\tilde{B}/B = O(10^{-4})$, but toroidal field ripple, other MHD modes or error fields may cause departures from axisymmetry.

The best fit to the amplitude data is obtained with the kinetic model. A likely explanation for this improved agreement is that the kinetic model treats dissipation more realistically than the resistive MHD models. This interpretation is consistent with stability analysis of the discharge. Calculations [16] and inferences from the burst cycle [20] indicate that the fast ion drive γ/ω is of $O(10^{-1})$. However, the continuum damping found by CASTOR is only $|\gamma/\omega| = 0.002$, so continuum damping is not an important dissipation mechanism. Calculations with NOVA-K that employed an MHD eigenfunction and perturbative calculations of Landau damping also could not explain the stability properties of the discharge [28]. In contrast, stability analysis with local, high-n models found that the 'radiative' damping rate is comparable to the fast ion drive and dominates over other damping mechanisms. Global (kinetic) PENN stability analysis also found good agreement between the observed stability threshold and the predicted threshold [12].

In summary, magnetic probe measurements are a useful diagnostic of the TAE. The best fit to the amplitude data is obtained with a kinetic model that includes Landau damping and finite Larmor radius effects.

ACKNOWLEDGEMENTS

Useful discussions with E. Carolipio, M. Chu, G. Huysmans, S. Sharapov, E. Strait, A. Turnbull and L. Villard are gratefully acknowledged. This work was supported by subcontract No. SC-L134501 to USDOE Contract No. DE-AC03-89ER51114, by the Swedish and the Swiss National Science Foundations, by the Nederlandsche Organisatie voor Wetenschappelijk Onderzoek and by the supercomputer centres in Lausanne and Linköping.

REFERENCES

[1] HEIDBRINK, W.W., in Theory of Fusion Plasmas (Proc. Joint Varenna–Lausanne Int. Workshop Varenna, 1994), Editrice Compositori, Bologna (1994) 49.
[2] WONG, K.L., et al., Phys. Rev. Lett. **76** (1996) 2286.
[3] FASOLI, A., et al., Phys. Rev. Lett. **76** (1996) 1067.
[4] NAZIKIAN, R., et al., Phys. Rev. Lett. **78** (1997) 2976.
[5] HEIDBRINK, W.W., et al., Phys. Fluids B **3** (1991) 3167.
[6] SESNIC, S., et al., Nucl. Fusion **33** (1993) 1877.
[7] DURST, R.D., et al., Phys. Fluids B **4** (1992) 3707.
[8] CHENG, C.Z., Phys. Fluids B **3** (1991) 2463.
[9] METT, R.R., MAHAJAN, S.M., Phys. Fluids B **4** (1992) 2885.
[10] CANDY, J., ROSENBLUTH, M.N., Nucl. Fusion **35** (1995) 1069.
[11] VLAD, G., ZONCA, F., ROMANELLI, F., Nucl. Fusion **35** (1995) 1651.
[12] JAUN, A., VACLAVIK, J., VILLARD, L., Phys. Plasmas **4** (1997) 1110.
[13] BRIGUGLIO, S., KAR, C., ROMANELLI, F., VLAD, G., ZONCA, F., Plasma Phys. Control. Fusion **37** (1995) A279.
[14] CHENG, C.Z., GORELENKOV, N.N., HSU, C.T., Nucl. Fusion **35** (1995) 1639.
[15] SANTORO, R.A., CHEN, L., Phys. Plasmas **3** (1996) 2349.
[16] STRAIT, E.J., HEIDBRINK, W.W., TURNBULL, A.D., CHU, M.S., DUONG, H.H., Nucl. Fusion **33** (1993) 1849.

[17] TURNBULL, A.D., et al., Phys. Fluids B **5** (1993) 2546.
[18] STRAIT, E.J., HEIDBRINK, W.W., TURNBULL, A.D., Plasma Phys. Control. Fusion **36** (1994) 1211.
[19] HEIDBRINK, W.W., STRAIT, E.J., CHU, M.S., TURNBULL, M.S., Phys. Rev. Lett. **71** (1993) 855.
[20] HEIDBRINK, W.W., et al., Phys. Fluids B **5** (1993) 2176.
[21] STRAIT, E.J., Rev. Sci. Instrum. **67** (1996) 2538.
[22] HUYSMANS, G.T.A., GOEDBLOED, J.P., KERNER, W., Phys. Fluids B **5** (1993) 1545.
[23] HUYSMANS, G.T.A., KERNER, W., BORBA, D., HOLTIES, H.A., GOEDBLOED, J.P., Phys. Plasmas **2** (1995) 1605.
[24] JAUN, A., APPERT, K., VACLAVIK, J., VILLARD, L., Comput. Phys. Commun. **92** (1995) 153.
[25] LAO, L.L., ST. JOHN, H., STAMBAUGH, R.D., KELLMAN, A.G., PFEIFFER, W.P., Nucl. Fusion **25** (1985) 1611.
[26] HUYSMANS, G.T.A., GOEDBLOED, J.P., KERNER, W., in Computational Physics (Proc. Conf. Singapore, 1990), World Scientific Publishing, Singapore (1991) 371.
[27] LÜTJENS, H., BONDESON, A., ROY, A., Comput. Phys. Commun. **69** (1992) 287.
[28] CHENG, C.Z., et al., in Plasma Physics and Controlled Nuclear Fusion Research 1994 (Proc. 15th Int. Conf. Seville, 1994), Vol. 3, IAEA, Vienna (1995) 373.
[29] METT, R.R., STRAIT, E.J., MAHAJAN, S.M., Phys. Plasmas **1** (1994) 3277.

(Manuscript received 23 January 1997
Final manuscript accepted 7 July 1997)

E-mail address of W.W. Heidbrink:
heidbrink@gav.gat.com

Subject classification: D3, Te